How relative defect migration energies drive contrasting temperature-dependent microstructural evolution in irradiated ceramics

Aurélien Debelle, Jean-Paul Crocombette, Alexandre Boulle, Enrique Martínez, Blas Pedro Uberuaga, Diana Bachiller-Perea, Yara Haddad, Frederico Garrido, Lionel Thomé, Moni Behar

How relative defect migration energies drive contrasting temperature-dependent microstructural evolution in irradiated ceramics

Aurélien Debelle*[1,2], Jean-Paul Crocombette[3], Alexandre Boulle[4], Enrique Martinez[5], Blas Pedro Uberuaga[5], Diana Bachiller-Perea[1], Yara Haddad[1], Frédérico Garrido[1], Lionel Thomé[1], Moni Béhar[6]

1. Centre de Sciences Nucléaires et de Sciences de la Matière (CSNSM), Université Paris-Sud, CNRS/IN2P3, Université Paris-Saclay, 91405 Orsay, France.
2. CEA, DEN, Service de Recherche de Métallurgie Physique (SRMP), Laboratoire JANNUS, Université Paris-Saclay, 91191 Gif-sur-Yvette, France.
3. CEA, DEN, Service de Recherche de Métallurgie Physique (SRMP), Université Paris-Saclay, 91191 Gif-sur-Yvette, France.
4. Institut de Recherche sur les Céramiques (IRCer), CNRS UMR 7315, Centre Européen de la Céramique, 12 rue Atlantis, 87068 Limoges, France.
5. Materials Science and Technology Division, Los Alamos National Laboratory, Los Alamos, New Mexico 87545, USA.
6. Instituto de Física, Universidade Federal do Rio Grande do Sul, C.P. 15051, 91501-970 Porto Alegre, RS, Brazil.

Abstract

Ceramic materials have become widely used in various fields of material science, and ceramic oxides such as cubic zirconia (c-ZrO_2) and magnesia (MgO) are candidate materials for nuclear energy applications. For the corresponding in-service conditions of these materials, there is a crucial need in studies at moderate or high temperatures of the physical phenomena underlying the damage build-up under irradiation. In the present work, we show, using X-ray diffraction, that these two materials exhibit similar damage accumulation process under ion irradiation at fixed temperature. However, they display an unexpected opposite damaging rate to changes in the irradiation temperature. In fact, as the temperature is increased, the final damage state is reached earlier in c-ZrO_2 while it is delayed in MgO. Rate equation cluster dynamics simulations show that defect clustering is favored over defect recombination in c-ZrO_2, but the situation is reversed for MgO, explaining the observed opposite response to temperature of the two materials. This contrasting behavior can be rationalized in terms of non-equivalent interstitial versus vacancy defect migration energies in MgO. We finally demonstrate that these results allow for a qualitative prediction of the evolution of the experimental irradiation-induced disorder with temperature, henceforth potentially reducing the cost in selecting and developing *ad hoc* materials.

*Corresponding author: aurelien.debelle@u-psud.fr

Keywords: irradiation; defect migration energy; X-ray diffraction; rate theory; disorder

I. Introduction

The modification of matter upon interaction with energetic particles arises through the transfer of energy from the incident particles to the atomic nuclei and/or to the electrons of the target [1]. This process, referred to as irradiation, may lead to defect generation and subsequent microstructural changes. These effects may have beneficial or detrimental implications in many fields of applied materials science such as advanced electro-optical devices [2-4], engineered nanostructures [5-7], strain engineering [8-10], nuclear materials [11-13] and space exploration [14,15]. The physical phenomena underlying the damage build-up under irradiation have been the focus of research for several decades, but there is still a need for comprehensive studies at moderate or high temperatures that correspond to most of the in-service conditions of actual relevance.

In the context of ceramics, important for many of the applications above, much work has focused on the behavior of materials that undergo amorphization upon irradiation. The effect of an increase in irradiation temperature on the threshold fluence (number of particles per unit surface) for such a phase change to occur has been particularly scrutinized in oxides and carbides. The primary observation was a delay or even a complete suppression of the amorphization process with increasing temperature owing to enhanced dynamic defect annealing (see e.g. these comprehensive papers [16-18]). In contrast, studies of the effect of temperature variation on the response of ceramics that retain their crystalline structure under irradiation are much scarcer [19-22]. Among these materials, cubic (yttria-stabilized) zirconia (c-ZrO_2) and magnesia (MgO), which have been examined over a wide temperature range, exhibit an opposite response in the temperature dependence of the irradiation-induced damage build-up [23,24]. This unexpected opposite behavior is the subject of the paper study.

Cubic zirconia and magnesia are two materials that have received particular attention, owing to their potential applications in nuclear energy (both fission and fusion) [25,26], and, in the case of zirconia, as solid oxide fuel cells for high-energy-density portable power supplies [27]. The two materials exhibit significant differences including the crystalline structure and the ionicity of the bonding (MgO having higher ionic character). In spite of these differences, at a fixed temperature, they

behave similarly under ion irradiation. In fact, in both materials, one observes a continuous damage accumulation process: this process starts with point defect creation and then, at a transition fluence, identified by Rutherford backscattering spectroscopy in channeling mode (RBS/C), the disorder increases as a result of the formation of extended defects (in majority of large dislocation loops) [23-24]; disorder finally culminates with the formation of a network of tangled dislocation lines [23,28]. The two materials do not undergo any phase change and they both retain their crystalline character. This process is the same irrespective of the temperature. However, the two materials display an unexpected opposite damage build-up rate to changes in the irradiation temperature [23,24]. Indeed, as partially demonstrated by RBS/C, as the temperature is increased, the accumulation of disorder is accelerated in c-ZrO_2 but it is retarded in MgO. The corresponding transition fluence at which this increase in damage occurs decreases with increasing temperature for c-ZrO_2, while it increases for MgO. This result is illustrated in Fig.1 of the Supplemental Material [29].

In the present work, we rationalize this strikingly opposite response of the two materials to the irradiation temperature and correlate it with the relative diffusivities of irradiation-created defects. X-ray diffraction (XRD) measurements indicate that in addition to the temperature dependence, there exists, in c-ZrO_2, two fluence regimes in which the material response differs. The experimental results are qualitatively reproduced using Rate Equation Cluster Dynamics (RECD) simulations which allow us to conclude that the key property leading to the different damage accumulation rates is a difference in the defect migration energies between vacancies and interstitials.

II. X-ray diffraction and rate equation cluster dynamics theoretical background

As one of the objectives of this study is to compare disorder parameters derived from XRD and RECD, a brief presentation of the theoretical background of both methods is mandatory to understand the meaning of the presented data.

XRD theory

The disorder, obtained from the fitting of the experimental data with the RaDMaX program [31], is the parameter of interest in this work. The XRD-derived disorder is linked to the so-called static Debye-Waller (DW) factor that damps the coherent scattered intensity due to the presence of defects in the crystalline lattice [32 and references therein]. This factor is expressed as follows:

$$\mathrm{DW} = \int d\mathbf{u} \cdot p(\mathbf{u}) \exp(i\mathbf{Q}\mathbf{u}) \quad (1)$$

where **Q** is the diffraction vector ($Q = 4\pi\sin\theta/\lambda$, with θ the diffraction angle). The displacement field consecutive to displaced atoms can be conveniently described with the vector **u**, where the displacement $\mathbf{u}_j$ at a given site *j* is determined by the probability distribution function (pdf), *p*(**u**), of the random variable **u**. The DW factor is thus the Fourier transform of *p*(u), i.e. its characteristic function. *p*(u) captures all the statistical information regarding atomic displacements. The DW factor parameter is therefore directly related to the nature, density and spatial distribution of the defects [32], and it also depends on the probed hkl reflection. It is important to understand that the DW factor does not correspond to absolute values of disorder, but rather that its evolution, from a perfect (DW=1) to a severely defective (DW$\rightarrow$0) crystal, provides a measure of the variation of the disorder level for a given system. In the following, we use the quantity $\langle(1\text{-DW})_{max}\rangle$ as a measure of the disorder level which has the advantage of increasing (from 0 to 1, by definition of the DW factor [32]), as the damage increases, hence simplifying the comparison with other measures of disorder (like the damage fraction commonly used in RBS/C).

RECD theory

In the present study, to perform rate equation cluster dynamics simulations, we used the 1D version of the CRESCENDO code, restricted to the case where only single defects are mobile in a homogeneous framework. A brief summary of the method is presented below, and the reader is referred to [33] and [34] for a complete description of the code and to a previous study [35] for a more detailed presentation of the simulation set-up. Focusing on interstitial clusters, which are of primary interest in this work, the evolution of the concentration $C(I_n)$ of clusters I_n containing *n* interstitials is driven by the difference in rate (*J*) of cluster growth from size I_{n-1} to I_n ($J_{I_{n-1}\rightarrow I_n}$) and in shrinkage from I_{n+1} to I_n ($J_{I_{n+1}\rightarrow I_n}$). Each rate is the sum of two contributions, corresponding to the interaction with mobile monointerstitials and monovacancies, respectively. For each mobile defect, there is an absorption component, governed by a factor β, and a thermal emission component, governed by a factor α. For example, the growth rate due to mobile interstitials reads:

$$J^{I}_{I_{n-1}\rightarrow I_n} = \beta_{n-1,I} C\left(I_{n-1}\right) C\left(I\right) - \alpha_{n,I} C\left(I_n\right) \tag{2}$$

The emission term depends only on the concentration of the immobile emitting species, whereas the absorption term depends on the concentrations of both the captured mobile and capturing immobile species. Importantly, β is expressed as [33]:

$$\beta_{n-1,I} = 4\pi Z_I D_I d_{I-I_{n-1}} \tag{3}$$

In Eq.(3), D_I is the diffusion coefficient of mono-interstitials which essentially depends on their migration energy and $d_{I-I_{n-1}}$ is the capture distance of an interstitial by a cluster of size *n-1*. The bias factor (Z_I = 1.1) accounts for elastic interactions (i.e. enhanced capture rate) between dislocations and mobile interstitials, and it has proven to be fundamental in the modelling of the evolution of irradiation defects [36-37]. The exact calculation of this bias factor involves complex calculations of elastic interactions [38] and is beyond the scope of the present paper.

Elastic interactions between dislocations and vacancies are comparatively negligible, thus the counterpart term does not appear in the corresponding equations (Z_v = 1) [36-37]. Finally, the equation governing the evolution of the mobile mono-interstitials is:

$$\frac{dC(I)}{dt} = G_I - \sum_{n>1} J^I_{I_n \to I_{n+1}} + \sum_{n>1} J^I_{V_n \to V_{n+1}} \\ +2\left(\alpha_{2,I} C(I_2) - \beta_{1,I} C(I) C(I)\right) - 4\pi (D_I + D_V) d_{I-V} C(I) C(V) - \rho Z_I D_I C(I) \quad (4)$$

with D_v the diffusion coefficient of mono-vacancies. ρ is the density of intrinsic sinks within the microstructure and hence, the last term in Eq. (4) denotes the elimination of mobile interstitials at dislocation or interfacial sinks. The first term in the right-hand-side of Eq. (4) is the source term which represents the production of defects by irradiation (see below). The penultimate term is the interstitial-vacancy recombination rate that depends on the sum of the diffusion coefficients of interstitials and vacancies. Note that the formation of di-interstitials has a special form, the factor 2 coming from the fact that both species that form the cluster are mobile. Finally, the remaining terms represent the reaction rates of interstitials with both interstitial and vacancy clusters.

III. Results and discussion

III.1. XRD experiments

Figure 1a shows the disorder level at the maximum of the damage profile (the profile is not flat because MeV ions do not have a constant energy-loss over their entire range) for irradiated c-ZrO_2 single crystals as a function of fluence at four temperatures: 80, 573, 773 and 1073 K. An increase in the disorder is observed with increasing fluence irrespective of the temperature. More interestingly, for all temperatures, two regimes can be identified. At low fluence, *i.e.* less than ~2-4x10^{14} cm^{-2}, the disorder decreases with increasing temperature, while it increases at greater fluences. This behavior is made clearer when comparing the values of disorder at two particular fluences indicated by the vertical dashed lines in the figure (the blue line at 2x10^{14} cm^{-2} and the red line at 10^{15} cm^{-2}). Values along these lines are plotted in Fig.2a. Clearly, the higher the temperature, the faster the final damage

state (i.e. when the disorder saturates) is reached. Note that in the present case complete disorder does not imply an amorphous structure: the samples retain their crystalline structure but the disorder (due to extended defects in the crystalline matrix) extinguishes the coherent part of the diffraction signal which is redistributed as diffuse scattering around the Bragg peaks. Such diffuse scattering clouds are readily observed in reciprocal space maps of irradiated c-ZrO_2 and MgO [23,24].

In contrast, Figure 1b shows the disorder level determined for irradiated MgO single crystals as a function of ion fluence for the same four temperatures as for c-ZrO_2. The investigated fluence range is smaller in MgO than it is in c-ZrO_2, but it does capture the entire disordering process up to saturation. We also note that the disorder levels found in MgO are different from those observed in c-ZrO_2, but as explained above and in [32], it is not meaningful to compare absolute values in different materials owing to the definition of the DW factor. Rather, it is the trend in the evolution of disorder with fluence that is relevant. The same trend is observed with varying temperature as we observe a progressive increase in disorder until complete disorder in all cases. Although the increase in disorder is monotonous, to compare with zirconia we identified low and high fluence regimes characteristic of MgO, as indicated by the two dashed lines in Fig. 1b at $9x10^{12}$ and $7.5x10^{13}$ cm^{-2}. In these two regimes, and as shown in Fig. 2b, the XRD-derived disorder decreases with increasing temperature irrespective of fluence. Therefore, similar to zirconia, the disorder in the low fluence regime decreases in magnesia with increasing temperature but, in contrast to c-ZrO_2, it also diminishes in the high fluence regime. That is, for all fluences, damage accumulation always decreases with increasing temperature in MgO, but not in c-ZrO_2. This is dramatically illustrated in Fig. 1, where the disorder curves at different temperatures cross as a function of fluence in c-ZrO_2 but do not cross in MgO, and in Fig. 2, where the curves both have negative slope in MgO but opposite slopes in c-ZrO_2. As a consequence, within experimental uncertainty, the final damage state reached at high fluence always occurs earlier for higher temperature irradiations in c-ZrO_2, in complete contrast to MgO (and despite similar defect evolution occurring in both materials at fixed temperature, as revealed by RBS/C and transmission electron microscopy - TEM [23-24,28]).

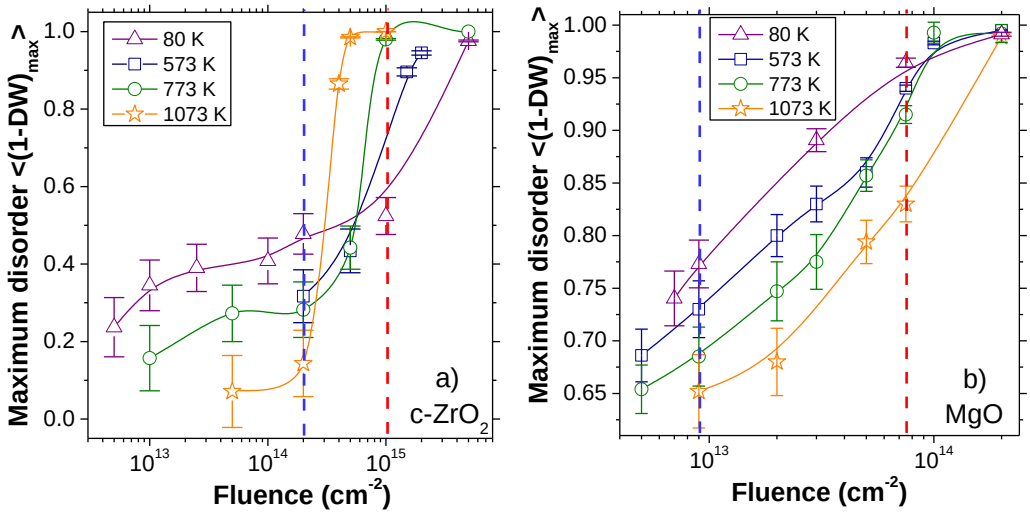

Figure 1: Disorder level averaged over a depth window centered on the peak of the irradiation damage profile. This disorder was determined by fitting the XRD θ-2θ scans reported in [23] for c-ZrO_2 and provided in Fig. 2 of the Supplementary Material [29] for MgO. Disorder is given as a function of ion fluence and temperature for a) c-ZrO_2 and b) MgO. In each figure, the blue dashed line indicates results representative of a low fluence regime while the red dashed line represents a high fluence regime.

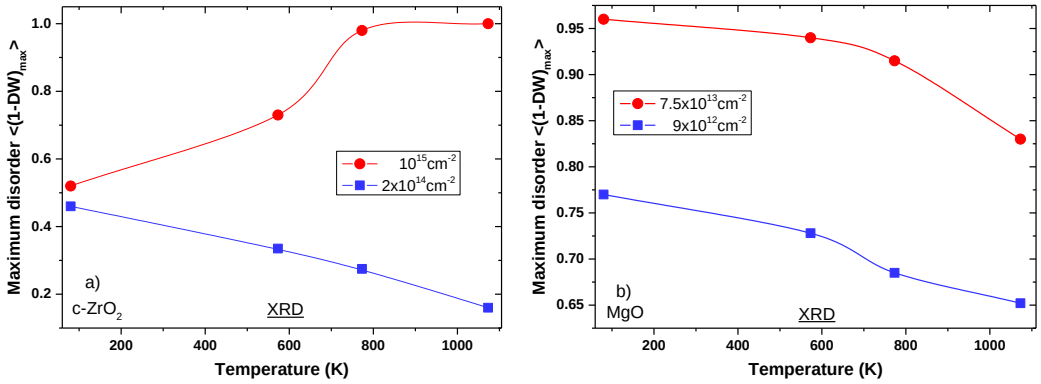

Figure 2: Disorder as determined from XRD experiments as a function of temperature, at low and high fluences characteristic of two regimes in the damage accumulation process (see Fig.1), in a) c-ZrO_2 and b) MgO.

Increasing temperature obviously leads to an increase in the defect mobility, but the final effect could be an enhanced clustering rate or an enhanced recombination rate. In previous work, we put forward the *hypothesis* that the origin of the contrasting behavior between c-ZrO_2 and MgO could result from a dominant clustering process in the former material versus a dominant recombination process in the latter [23,24]. Guided by this assumption, we developed a RECD model to determine the

impact of the defect migration energetics on the evolution of the defect distributions in the two materials. RECD results are presented in the next section.

III.2. RECD simulations

In order to apply the RECD framework to c-ZrO_2 and MgO, we had to make, rooted in the properties of zirconia, some simplifying assumptions that are discussed in what follows. First, we approximated the source term by a creation of monovacancies (V) and monointerstitials (I), which is justified by molecular dynamics simulations that indicated that the majority of the defects formed in a collision cascade in these materials are precisely point defects [39-40]. The rate of defect creation was determined from SRIM [41] calculations using 40 eV and 55 eV as threshold displacement energies for both sublattices (which are commonly used in the literature) for c-ZrO_2 and MgO, respectively. It is known that this code overestimates the rate of surviving defects (because for instance it does not consider intra-cascade recombination) [42,43]. A recent quantitative study of irradiation defects in MgO as a function of temperature indicates that the actual defect creation efficiency is in the range of a few percent; we hence divided the SRIM-predicted values by a factor of 10. Defect creation fluxes were then $4x10^{18}$ $cm^{-3}.s^{-1}$ for c-ZrO_2 and $1.9x10^{18}$ $cm^{-3}.s^{-1}$ for MgO. Second, as we could only treat one sublattice, we considered only the cationic sublattice in c-ZrO_2 because cations in this material (like in UO_2) are the rate limiting species in the diffusion processes (and also because of the large concentration of intrinsic vacancies in stabilized zirconia). Likewise, as in MgO the properties of both anion and cation defects are very similar [44], there is no loss in generality just considering the cations, and that is what we did. Based on the data reported in the literature, we used the following values for the defect migration energies: 3 eV for both V and I in c-ZrO_2 [45,46], and 2 and 0.4 eV for V and I, respectively, in MgO [41,47]. Note that the value of 3 eV for c-ZrO_2 is a lower limit of values reported in the literature (all obtained with empirical potentials). Values of 5-6 eV are typically reported but, with such high values, defect migration is hampered below high temperature (> 1500 K) and therefore, RECD simulations did not show any significant variation in the calculated parameters (i.e. reaction rates and disorder level, see section III). There are thus two differences in the defect diffusivity between the

two materials: (i) defect mobility is larger in MgO than in c-ZrO_2 for both I and V defects and, most critically, (ii) the relative mobility of V and I is very different in MgO but is similar in c-ZrO_2. We want to emphasize that, except the rate at which defects are created, the only major difference between the models for c-ZrO_2 and MgO is the defect migration energies.

Our first RECD calculations dealt with the determination of two reaction rates for both materials at different fluences for a wide range of temperatures: the recombination (rec) rate between I and V, and the interstitial clustering (clust) rate (see Eq.(3)). As noted, these are the two rates hypothesized to be very different for the two materials (and the elimination rate was verified to be significantly lower). We analyzed only the clustering of interstitials because it has been shown that these defects are the major source of the irradiation disorder, as evidenced by numerous RBS/C and XRD results [23-24,28 and references therein] (to be clear, migration processes related to vacancies were also considered in the calculations, these were just not analyzed in any detail). Figure 3a shows the two rates determined for c-ZrO_2 at two fluences, $1.5x10^{14}$ cm^{-2} and $1.5x10^{15}$ cm^{-2} (these fluences are characteristic of the two regimes determined experimentally and defined by the vertical dashed lines in Fig. 1a). The defect source term is also given for comparison. It can be observed that, for temperatures for which significant variations are observed (i.e. $\gtrsim$ 1000 K), the clustering rate is almost constant but more importantly, it is larger than the rate for defect recombination. These data hence support our hypothesis of favored defect clustering in c-ZrO_2. Furthermore, this hypothesis allows explaining the early transition in the damage accumulation process observed experimentally in this material (see Fig. 1a) as this transition, as previously explained, arises from the clustering of small-scale defects to form extended defects. The corresponding reaction rates for MgO are given in Fig. 3b for the two characteristic fluences of $5x10^{12}$ cm^{-2} and $5x10^{13}$ cm^{-2}. There are bigger changes in these rates at a lower temperature than for c-ZrO_2 (due to the lower defect migration energies). Note the logarithmic Y-scale which indicates a large range in the defect clustering rate *vs* temperature. The rate of defect clustering is much smaller than that for defect recombination for both fluences, again in

support of the hypothesis put forward earlier. More importantly, it decreases with increasing temperature, explaining the delay in the transition fluence in the disorder accumulation process.

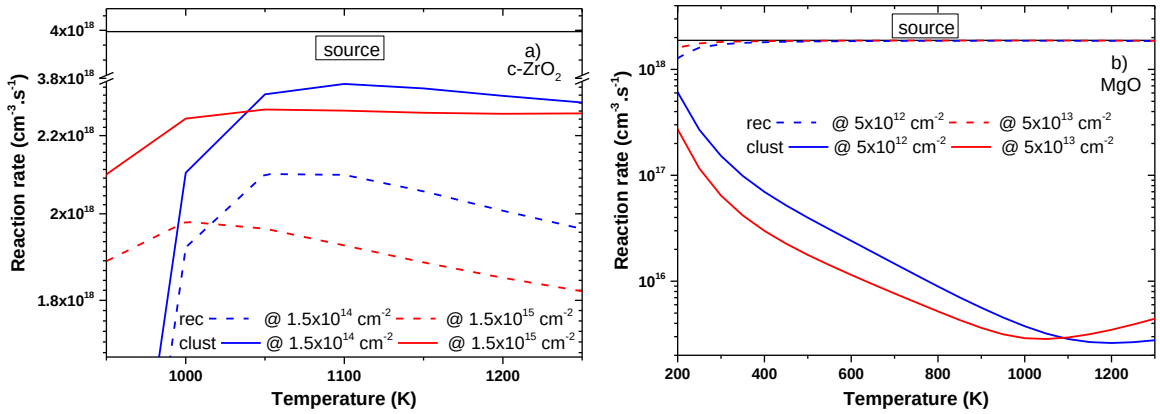

Figure 3: Source term for defect generation (horizontal black solid lines) and recombination (rec, dashed lines) and clustering (clust, solid lines) reaction rates as determined from RECD simulations as a function of temperature for a) c-ZrO_2 and b) MgO, at both low and high fluences characteristic of the two regimes experimentally identified in the damage accumulation process (see Figs. 1a and 1b).

As highlighted in Eq. (3), the terms appearing in the evolution of mono-defects can be divided into three parts: clustering, elimination, and recombination rates. The first two terms depend only on the diffusion coefficient of the relevant mono-defect while recombination depends on the sum of both (I and V) diffusion coefficients. Furthermore, the clustering term involves, for interstitials, a bias term (Z_I = 1.1 in Eq. (2)). Considering these equations, it can be observed that, for c-ZrO_2, since the mobilities of vacancies and interstitials are identical, the difference in the clustering and recombination rates is only due to this bias factor, which explains why the Y-scale is limited. More importantly, in MgO, interstitials are mobile well before vacancies are and, therefore, the probability for a mono-interstitial to meet a mono-vacancy is high at low temperature because the concentration of the latter is large, a consequence of the fact that their mobility is low and thus they can neither cluster nor eliminate at sinks. The recombination rate is therefore very high. As the recombination process takes place, the concentration of interstitials C_I drastically decreases and so does the clustering rate, explaining why it varies over several decades in MgO. However, such a huge decrease in the clustering rate does not

imply that extended defects, such as dislocation loops, do not form (they actually do form, just at a slower effective rate than in c-ZrO_2).

III.3. Direct comparison between XRD experiments and RECD simulations

The RECD simulations conclusively show that the existence or not of a difference in I and V mobility plays a crucial role in the defect accumulation process in irradiated c-ZrO_2 and MgO over a large range of temperatures, resulting in different dominating defect reaction processes in the two materials: enhanced defect clustering in the former and preferential defect recombination in the latter. However, the key question is whether these reactions are responsible for the contrasting evolution in the damage build-up as a function of the temperature and fluence for the two materials. To answer this question, we identified a disorder parameter obtained with RECD calculations that could be compared to the disorder level derived from the XRD measurements. It is known that, in the two fluence regimes identified in this work for both materials, dislocation loops are the main defects formed [23-24,28,48-49 and references therein]. Theory of diffuse scattering from dislocation loops indicates that the DW factor is proportional to the dislocation loop density times the number of point defects in the loops to the 3/2 power [50]. Therefore, the disorder parameter determined from the RECD calculations was computed as follows:

$$\sum_m c_m^l m^{3/2} \quad (5)$$

c_m^l being the volume density of dislocation loops of size *m* where *m* is the number of interstitials inside each of the loops.

The RECD-derived disorder in c-ZrO_2, as a function of temperature, is shown in Fig.4a. As was done for the analysis of the experiments, two fluences characteristic of the different damage accumulation regimes have been examined. Qualitative agreement is found when comparing this computed disorder with the XRD-derived disorder (see Fig. 2a). Importantly, the two distinct and opposite dependencies of disorder on temperature for both fluences are reproduced by our RECD model. The RECD-derived disorder as a function of the temperature for MgO is presented in Fig.4b.

Experiments indicated a continuous decrease in the disorder level with increasing temperature, irrespective of the fluence regime (see Fig. 2b). This behavior is reproduced in the RECD simulations. In addition, the temperature range over which significant evolution in the disorder is observed agrees reasonably well between experiments and simulations, providing some confidence that the RECD model is indeed capturing the relevant physical behavior of the defects. Also important is the fact that using, in Eq. (4), a power lower than 3/2 did not provide satisfactory results, meaning that the disorder parameter is governed by a collective process affected by both loop density and size.

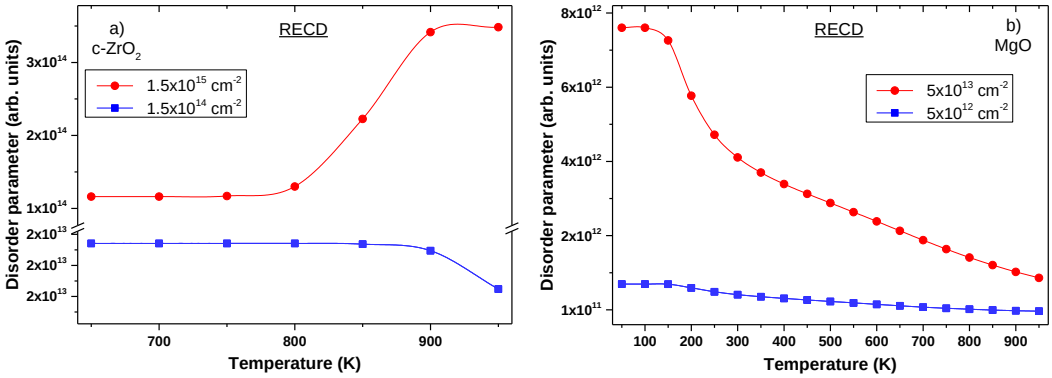

Figure 4: Disorder as determined by RECD simulations as a function of temperature at low and high fluences characteristic of two regimes in the damage accumulation process (see Fig.1), in a) c-ZrO_2 and b) MgO.

The RECD calculations presented in this work contain a number of assumptions, including homogenous defect distributions, neutral defects (no electrostatic interactions), and immobile defect clusters. In spite of these assumptions, they provide an explanation for the opposite response in terms of damage build-up under irradiation with increasing temperature of the two studied materials. Furthermore, they reproduce the experimentally-observed dependencies of the evolution of radiation-induced disorder (and associated microstructural changes) on both fluence and irradiation temperature. The key parameters in the calculations, the defect migration energies, are shown to directly govern the relative contribution of clustering and recombination reaction rates. More precisely, we showed that the dominant mechanism depends on the relative mobility of interstitials versus vacancies. In c-ZrO_2, the mobility of these two defects is similar, and thus, independent of the irradiation temperature, defect clustering is favored over defect recombination due to the inherent elastic attraction of mobile interstitials to dislocation loops. In contrast, in MgO, the relative immobility

of vacancies as compared to interstitials results in recombination dominating over clustering and, above all, to a decrease in the clustering rate with temperature. From these results, we can rationalize the response of these two materials and explain why the damage accumulation is delayed in MgO but is accelerated in c-ZrO_2 when the irradiation temperature is increased.

This study highlights the fact that the role of temperature during irradiation is definitely non-trivial, a consequence of the widely-varying rates of processes that compete at the atomic scale. Indeed, except when cavities (voids and bubbles) are involved, an increase in temperature is usually assumed to lead to an enhancement of dynamic annealing and therefore to a significant slowing-down in the damage accumulation process. This is the case for e.g. silicon carbide (SiC) [51] and strontium titanate (STO) [52] in which there exists significantly different defect mobilities, (see [53] and [54], for SiC and STO, respectively). However, as shown in this work, depending on the defect energetics, irradiation-induced microstructural changes can on the contrary be accelerated. That is, temperature can exacerbate certain damage accumulation processes in some materials. This should occur in uranium dioxide and other fluorite-structured materials for instance, because the mobility of I and V defects is similar [55]. This prediction has been very recently verified experimentally. Indeed, RBS/C measurements (shown in the Supplemental Material [29]) have been performed on Ce-irradiated UO_2 at both room-temperature and 773 K, showing that just as for c-ZrO_2, the final microstructural state is reached at lower fluence with increasing the temperature.

IV. Conclusion

In this study, we used XRD to determine the evolution of the disorder in c-ZrO_2 and MgO upon ion irradiation as a function of both the ion fluence and the irradiation temperature. We observed that, at a fixed temperature, the two materials exhibit a similar response in terms of damage accumulation and microstructural changes (with an additional dependence on ion fluence for c-ZrO_2). However, strikingly, the rate of these changes is completely opposite when the temperature is changed. In fact, the final damage state is reached faster in c-ZrO_2 and is delayed in MgO when the temperature is increased. By performing RECD simulations, we provide an answer to this intriguing result. As is well established, the microstructural evolution of irradiated materials is driven by the defect diffusivity. However, the relative defect-migration energies of interstitial versus vacancy defects drive the temperature-dependent behavior. It can thus be concluded that disparities in defect mobilities can lead to very different responses to irradiation. For instance, a large difference in the I versus V diffusivity leads to an enhanced defect dynamic annealing. Finally, we propose an approximate yet revealing methodology, combining experiments and calculations, for the characterization, modeling and prediction of irradiation-induced disorder.

Acknowledgements

Several tens of crystals have been irradiated in order to perform all the experiments, and we are grateful to the SEMIRAMIS staff of the CSNSM for their constant help for the samples' irradiation. A.D. and J.-P.C. are indebted to Th. Jourdan for his precious help in the use of the CRESCENDO code. Part of this work has been funded by the NEEDS-Matériaux program of the CNRS. BPU was supported by the U.S. Department of Energy, Office of Science, Basic Energy Sciences, Materials Sciences and Engineering Division. Los Alamos National Laboratory, an affirmative action equal opportunity employer, is operated by Los Alamos National Security, LLC, for the National Nuclear Security Administration of the U.S. DOE under contract DE-AC52-06NA25396.

References

[1] M. Nastasi, J. W. Mayer, J. K. Hirvonen, Ion-solid interactions: fundamentals and applications, Cambridge University Press Eds, Cambridge (1996)

[2] H. C. Huang, J. I. Dadap, G. Malladi, I. Kymissis, H. Bakhru, R. M. Jr Osgood, Helium-ion-induced radiation damage in LiNbO3 thin-film electro-optic modulators, Opt. Express 22, 19653 (2014)

[3] N. Theodoropoulou, A. F. Hebard, M. E. Overberg, C. R. Abernathy, S. J. Pearton, S. N. G. Chu, R. G. Wilson, Unconventional Carrier-Mediated Ferromagnetism above Room Temperature in Ion-Implanted (Ga, Mn)P:C, Phys. Rev. Lett. 89, 107203 (2002)

[4] A. Redondo-Cubero, K. Lorenz, S. Magalhães, E. Alves et al., Analysis of the stability of InGaN/GaN multiquantum wells against ion beam intermixing", Nanotechnology 26, 425703 (2015)

[5] T. Som, D. Kanjilal, Nanofabrication by Ion-Beam Sputtering: Fundamentals and Applications, CRC Press, Taylor and Francis Group (2012)

[6] N. Yao, Focused Ion Beam Systems, MaterialsToday **10**, 53 (2007)

[7] Y. Zhang, M. Ishimaru, T. Varga, T. Oda, C. Hardiman, H. Xue, et al., Nanoscale engineering of radiation tolerant silicon carbide, Phys Chem Chem Phys. **14**, 13429 (2012)

[8] D. V. Potapenko, Z. Li, J. W. Kysar, R. M. Osgood, Nanoscale strain engineering on the surface of a bulk TiO_2 crystal, Nanoletters **14**, 6185 (2014)

[9] R. Gupta, N. Sehdev, K. Asokan, D. Kanjilal, S. Annapoorni, Engineering strain, densification, order parameter and magnetic properties of FePt thin films by dense electronic excitations, J. Appl. Phys. **116**, 083902 (2014)

[10] H. Guo, S. Dong, Ph. D. Rack, J. D. Budai, Ch. Beekman, Z. Gai, W. Siemons, C. M. Gonzalez, R. Timilsina, A. T. Wong, A. Herklotz, P. C. Snijders, E. Dagotto, Th. Z. Ward, Strain Doping: Reversible Single-Axis Control of a Complex Oxide Lattice via Helium Implantation, Phys. Rev. Lett **114**, 256801 (2015)

[11] Y. H. Li, B. P. Uberuaga, C. Jiang, S. Choudhury, J. A. Valdez, M. K. Patel, J. Won, Y.-Q. Wang, M. Tang, D. J. Safarik, D. D. Byler, K. J. McClellan, I. O. Usov, T. Hartmann, G. Baldinozzi, K. E. Sickafus, Role of Antisite Disorder on Preamorphization Swelling in Titanate Pyrochlores, Phys. Rev. Lett **108**, 195504 (2012)

[12] G. S. Was, Z. Jiao, E. Getto, K. Sun, A. M. Monterrosaa, S. A. Maloy, O. Anderoglu, B. H. Sencer, M. Hackett, Emulation of reactor irradiation damage using ion beams, Scripta Mater. **88**, 33 (2014)

[13] N. M. Anoop Krishnan, B. Wang, Y. Yu, Y. Le Pape, G. Sant, M. Bauchy, Phys. Rev. X **7**, 031019 (2017)

[14] A. Mozumder, Y. Hatano, Charged Particle and Photon Interactions with Matter: Chemical, Physicochemical, and Biological Consequences with Applications (chapter 4), Marcel Dekker Inc Eds, New York (2004)
[15] S. J. Pearton, F. Ren, E. Patrick, M. E. Law, A. Y. Polyakov, Ionizing Radiation Damage Effects on GaN Devices, ECS Journal of Solid State Science and Technology **5**, Q35 (2016)
[16] Y. Zhang, J. Lian, C. M. Wang, W. Jiang, R. C. Ewing, and W. J. Weber, Ion-induced damage accumulation and electron-beam-enhanced recrystallization in $SrTiO_3$, Phys. Rev. B **72**, 094112 (2005)
[17] E. Wendler, Th. Bierschenk, W. Wesch, E. Friedland, J. B. Malherbe, Temperature dependence of damage formation in Ag ion irradiated 4H-SiC, NIM B **268**, 2996 (2010)
[18] J. Lian, L.M. Wang, K. Sun, R. C. Ewing, In Situ TEM of Radiation Effects in Complex Ceramics, Microsc. Res. Techn. **72**, 165 (2009)
[19] P. Kalita, S. Ghosh, G. Sattonnay, U. B. Singh, V. Grover, R. Shukla, S. Amirthapandian, R. Meena, A. K. Tyagi, D. K. Avasthi, Role of temperature in the radiation stability of yttria stabilized zirconia under swift heavy ion irradiation: A study from the perspective of nuclear reactor applications, J. Appl. Phys. **122**, 025902 (2017)
[20] L. Vincent, L. Thomé, F. Garrido, O. Kaitasov, and F. Houdelier, Microstructure of Cs-implanted zirconia: Role of temperature, J. Appl. Phys. **104**, 114904-8 (2008)
[21] D. W. Clark, S. J. Zinkle, M. K. Patel, C. M. Parish, High temperature ion irradiation effects in MAX phase ceramics, Acta Mater. **105**, 130 (2016)
[22] C. Onofri, C. Sabathier, H. Palancher, G. Carlot, S. Miro, Y. Serruys, L. Desgranges, M. Legros, Evolution of extended defects in polycrystalline UO2 under heavy ion irradiation: combined TEM, XRD and Raman study, NIM B **374**, 51 (2016)
[23] A. Debelle, J. Channagiri, L. Thomé, B. Décamps, A. Boulle, S. Moll, F. Garrido, M. Behar, J. Jagielski, Comprehensive study of the effect of the irradiation temperature on the behavior of cubic zirconia, J. Appl. Phys **115**, 183504 (2014)
[24] D. Bachiller-Perea, A. Debelle, L. Thomé, M. Behar, Damage accumulation in MgO irradiated with MeV Au ions at elevated temperatures', J. Nucl. Mater. **478**, 268 (2016)
[25] C. Degueldre, Zirconia inert matrix for plutonium utilisation and minor actinides disposition in reactors, J. Alloys and Comp. **444/445**, 36 (2007)
[26] R.R. Macdonald, M.J. Driscoll, Magnesium oxide: An improved reflector for blanket-free fast reactors, Trans. Am. Nucl. Soc. **102**, 488 (2010)
[27] E. Fabbri, D. Pergolesi, E. Traversa, Ionic conductivity in oxide heterostructures: the role of interfaces, Sci Technol Adv Mater. **11**, 054503 (2010)
[28] S. Moll, Y. Zhang, A. Debelle, L. Thomé, J.P. Crocombette, Z. Zihua, J. Jagielski, W.J. Weber, Damage processes in MgO irradiated with medium-energy heavy ions, Acta Mater. **88**, 314 (2015)

[29] Supplemental Material
[30] C.-O. Bacri, C. Bachelet, C. Baumier, J. Bourçois, L. Delbecq, D. Ledu, N. Pauwels, S. Picard, S. Renouf, C. Tanguy, Nucl. Instr. Meth. B, in press, https://doi.org/10.1016/j.nimb.2017.03.036
[31] M. Souilah, A. Boulle, A. Debelle, RaDMaX: a graphical program for the determination of strain and damage profiles in irradiated crystals, J. Appl. Cryst. **49**, 311 (2016)
[32] A. Boulle, A. Debelle, Statistical nature of atomic disorder in irradiated crystals, Phys. Rev. Lett. **116**, 245501 (2016)
[33] T. Jourdan, G. Bencteux, G. Adjanor, Efficient simulation of kinetics of radiation induced defects: A cluster dynamics approach, Journal of Nuclear Materials **444**, 298 (2014)
[34] T. Jourdan, G. Stoltz, F. Legoll, L. Monasse, An accurate scheme to solve cluster dynamics equations using a Fokker-Planck approach, Comp. Phys. Comm. **207**, 170 (2016)
[35] S. Pellegrino, J.-P. Crocombette, A. Debelle, Th. Jourdan, L. Thomé, Multi-scale simulation of the experimental response of ion-irradiated zirconium carbide: Role of interstitial clustering, Acta Mater. 102, **79** (2016)
[36] P. T. Heald, M.V. Speight, Point-defect behavior in irradiated materials, Acta Metal. 23, 1389 (1975)
[37] T. Jourdan, Influence of dislocation and dislocation loop biases on microstructures simulated by rate equation cluster dynamics, J. Nucl. Mater. **467**, 286 (2015)
[38] D. Carpentier, T. Jourdan, Y. Le Bouar, M. C. Marinica, Effect of saddle point anisotropy of point defects on their absorption by dislocations and cavities, Acta Mater. **136**, 323 (2017)
[39] E. Zarkadoula, R. Devanathan, W. J. Weber, M. Seaton, I. T. Todorov, K. Nordlund, M. T. Dove, K. Trachenko, High-energy radiation damage in zirconia: Modeling results, J. Appl. Phys. **115**, 083507(2014)
[40] J.F. Ziegler, J. P. Biersack, U. Littmark, The Stopping and Range of Ions in Solids , Pergamon, New York, 1985. Available at: www.srim.org
[41] B. P. Uberuaga, R. Smith, A. R. Cleave, G. Henkelman, R. W. Grimes, A. F. Voter, K. E. Sickafus, Dynamical simulations of radiation damage and defect mobility in MgO, Phys. Rev. B **71**, 104102 (2005)
[42] R. S. Averback, R. Benedek, K. L. Merkle, Ion-irradiation studies of the damage function of copper and silver, Phys. Rev. B 18 (1978) 4156
[43] J.-P. Crocombette , L. Van Brutzel, D. Simeone, L. Luneville, Molecular dynamics simulations of high energy cascade in ordered alloys: Defect production and subcascade division, J. Nucl. Mater. 474, 134 (2016)
[44] B. P. Uberuaga, R. Smith, A. R. Cleave, F. Montalenti, G. Henkelman, R. W. Grimes, A. F. Voter, K. E. Sickafus, Structure and mobility of defects formed from collision cascades in MgO, Phys. Rev. Lett. **92**, 115505 (2004)

[45] M. Kilo, R. A. Jackson, G. Borchardt, Computer modelling of ion migration in zirconia, Phil. Mag. **83**, 3309 (2003)
[46] D. S. Aidhy, Y. Zhang, W. J. Weber, Radiation damage in cubic ZrO_2 and yttria-stabilized zirconia from molecular dynamics simulations, Scripta Mater. **98**, 16 (2015)
[47] C. A. Gilbert, S. D. Kenny, R. Smith, E. Sanville, Ab initio study of point defects in magnesium oxide, Phys. Rev. B **76**, 184103 (2007)
[48] A. Bhuian, K. Kuwahara,T. Yamamoto, K. Yasuda, S. Matsumura, H. Yasuda, Temperature dependent evolution of dislocation loops in YSZ under high energy electron irradiation, Trans. Mater. Res. Society of Japan **41**, 319 (2016)
[49] T. Sonoda, H. Abe, Ch. Kinoshita, H. Naramoto, Formation and growth process of defect clusters in magnesia under ion irradiation, Nucl Instr Meth Phys Res B **127**, 176 (1997)
[50] P. H. Dederichs, The theory of diffuse x ray scattering and its application to the study of point defects and their clusters, J. Phys. F: Metal Phys. **3**, 471 (1973)
[51] E. Wendler, Th. Bierschenk, W. Wesch, E. Friedland, J. B. Malherbe, Temperature dependence of damage formation in Ag ion irradiated 4H-SiC, Nucl. Instrum. Meth. B **268**, 2996 (2010)
[52] Y. Zhang, C. M. Wang, M. H. Engelhard, W. J. Weber, Irradiation behaviour of $SrTiO_3$ at temperatures close to the critical temperature for amorphization, J. Appl. Phys. **100**, 113533 (2006)
[53] M.-J. Zheng, N. Swaminathan, D. Morgan, I. Szlufarska, Energy barriers for point-defect reactions in 3C-SiC, Phys. Rev. B **88**, 054105 (2013)
[54] J. Won, L. J. Vernon, A. Karakuscu, R. M. Dickerson, M. Cologna, R. Raj, Y. Wang, S. Jo Yoo, S.-H Lee, A. Misra, B. P. Uberuaga, The role of non-stoichiometric defects in radiation damage evolution of $SrTiO_3$, J. Mater. Chem. A **1**, 9235 (2013)
[55] B. Dorado, D. A. Andersson, Ch. R. Stanek, M. Bertolus, B. P. Uberuaga, G. Martin, M. Freyss, Ph. Garcia, First-principles calculations of uranium diffusion in uranium dioxide, Phys. Rev. B **86**, 035110 (2012)